ARTICLES

Crystal structure of a bacterial homologue of Na^+/Cl^--dependent neurotransmitter transporters

Atsuko Yamashita[1], Satinder K. Singh[1], Toshimitsu Kawate[1], Yan Jin[2] & Eric Gouaux[1,2]

Na^+/Cl^--dependent transporters terminate synaptic transmission by using electrochemical gradients to drive the uptake of neurotransmitters, including the biogenic amines, from the synapse to the cytoplasm of neurons and glia. These transporters are the targets of therapeutic and illicit compounds, and their dysfunction has been implicated in multiple diseases of the nervous system. Here we present the crystal structure of a bacterial homologue of these transporters from *Aquifex aeolicus*, in complex with its substrate, leucine, and two sodium ions. The protein core consists of the first ten of twelve transmembrane segments, with segments 1–5 related to 6–10 by a pseudo-two-fold axis in the membrane plane. Leucine and the sodium ions are bound within the protein core, halfway across the membrane bilayer, in an occluded site devoid of water. The leucine and ion binding sites are defined by partially unwound transmembrane helices, with main-chain atoms and helix dipoles having key roles in substrate and ion binding. The structure reveals the architecture of this important class of transporter, illuminates the determinants of substrate binding and ion selectivity, and defines the external and internal gates.

Communication between neurons in the brain is critically dependent on the transmission of nerve impulses through chemical synapses, junctions at which electrical signals are relayed from one neuron to another via classical[1] neurotransmitters such as serotonin, norepinephrine, dopamine, glycine and GABA (γ-aminobutyric acid). Arrival of an action potential at the presynaptic terminal triggers release of these small molecules, which can then activate either millisecond-acting, ligand-gated ion channels or more slowly acting G-protein-coupled receptors[1]. After release and receptor activation, these neurotransmitters are actively cleared from the synapse primarily by specific, high-affinity integral membrane transporters located on the presynaptic terminal and surrounding glial cells. This energy-driven re-uptake not only returns synaptic neurotransmitter concentrations to basal levels but also allows for the replenishment of neurotransmitter stores in the lumen of presynaptic secretory vesicles by a separate class of vesicular carriers[2].

Na^+/Cl^--dependent transporters, also referred to as neurotransmitter sodium symporters (NSS), use sodium and chloride electrochemical gradients to catalyse the thermodynamically uphill movement of a wide array of substrates, including the biogenic amines (serotonin, dopamine, norepinephrine), amino acids (GABA, glycine, proline, taurine) and osmolytes (betaine, creatine)[2]. NSS members are distinct, in terms of amino acid sequence and functional properties, from the high-affinity, sodium-dependent glutamate transporters—the second major family of plasma membrane neurotransmitter transporters[2]. Dysfunction of Na^+/Cl^--dependent transporters contributes to multiple disorders, including depression[3], Parkinson's disease[3], orthostatic intolerance[3] and epilepsy[4]. Notably, they are the target of addictive substances such as cocaine and amphetamine[5] as well as therapeutic agents such as anticonvulsants[6] and the selective serotonergic re-uptake inhibitors[7].

A breakthrough in the structure/function analysis of Na^+/Cl^--dependent transporters occurred in the early 1990s, when the gene encoding the rat GABA transporter type 1 (GAT1)[8], along with other family members[9,10], was cloned. Analysis of the predicted amino acid sequences provided evidence for 12 transmembrane segments (TMs), with the amino and carboxy termini residing in the cytoplasm—predictions that were later confirmed by experiment[11]. Subsequent studies implicated residues in inhibitor recognition, substrate specificity, gating and ion binding. Crucial residues include a strictly conserved tyrosine in TM3 that is indispensable for substrate binding and transport[12,13], a position in TM1 occupied by either an aspartate or glycine, partially responsible for distinguishing between monoamine and amino acid substrates, respectively[10], and a negatively charged residue in extracellular loop 5 (EL5)/TM10 that is postulated to comprise part of an external gate[14] (Fig. 1a). Sodium:chloride:substrate stoichiometries have also been elaborated and vary from 1:1:1, 2:1:1 to 3:1:1 among different transporters[15–17]. At the present time, however, there is no structural paradigm for the interpretation of this wealth of functional data. Furthermore, there is no information, at the level of atomic detail, on the molecular principles underlying sodium-ion selectivity, sodium ion–substrate coupling and transport mechanism.

To obtain atomic resolution structural data on an NSS family member, we exploited the fact that prokaryotic organisms harbour NSS homologues[9,18]. Clusters of high sequence conservation, including functionally important residues, are distributed throughout the primary structure, although the overall sequence identity between the eukaryotic and prokaryotic counterparts is only 20–25% (Fig. 1a). Here we present the crystal structure of a bacterial homologue from *Aquifex aeolicus* ($LeuT_{Aa}$) and the molecular insights it unveils about the family of Na^+/Cl^--dependent neurotransmitter transporters.

Structure determination

$LeuT_{Aa}$ yielded crystals readily, and initial phases were determined by multiwavelength anomalous dispersion (MAD)[19] using a single

[1]Department of Biochemistry and Molecular Biophysics and [2]Howard Hughes Medical Institute, Columbia University, 650 West 168th Street, New York, New York 10032, USA.

crystal grown from selenomethionine-labelled protein and diffraction data measured to Bragg spacings of 1.9 Å (Supplementary Table 1). The resultant electron density map was unambiguous over almost the entire molecule. An initial model derived from automatic tracing was subjected to rounds of manual rebuilding and crystallographic refinement using a native data set to 1.65 Å resolution. The final model contains residues 5–133 and 135–513 of $LeuT_{Aa}$, leucine, two sodium ions, a chloride ion, five detergent molecules and 210 water molecules (Table 1).

Transporter architecture

The $LeuT_{Aa}$ protomer resembles a shallow 'shot glass', with the opening facing the extracellular space, the base facing the cytoplasm, and the bottom of the 'glass' located ~6 Å into the bilayer-spanning portion of the transporter (Fig. 2a, b). In the current structure there are no solvent-accessible channels traversing the membrane-spanning portion of the protein. The protomer is ~70 Å tall and ~48 Å in diameter and comprises 12 transmembrane helical regions (TM1 to TM12), together with numerous loops and helices on the intracellular and extracellular surfaces. To the best of our knowledge, the fold of $LeuT_{Aa}$ is not similar to that of any previously reported membrane protein structure.

There is an unanticipated internal structural repeat in the first ten transmembrane helices of the $LeuT_{Aa}$ protomer, relating TM1–TM5 and TM6–TM10 by a pseudo-two-fold axis located in the plane of the membrane (Figs 1b and 2c). Specifically, the α-carbon atoms of the 130 residues comprising helices TM1–TM5 can be superposed onto those from TM6–TM10 by a rotation of 176.5°, yielding a root mean square deviation (r.m.s.d.) of 5.3 Å. This approximate symmetry is not detectable in the amino acid sequence, and it positions the

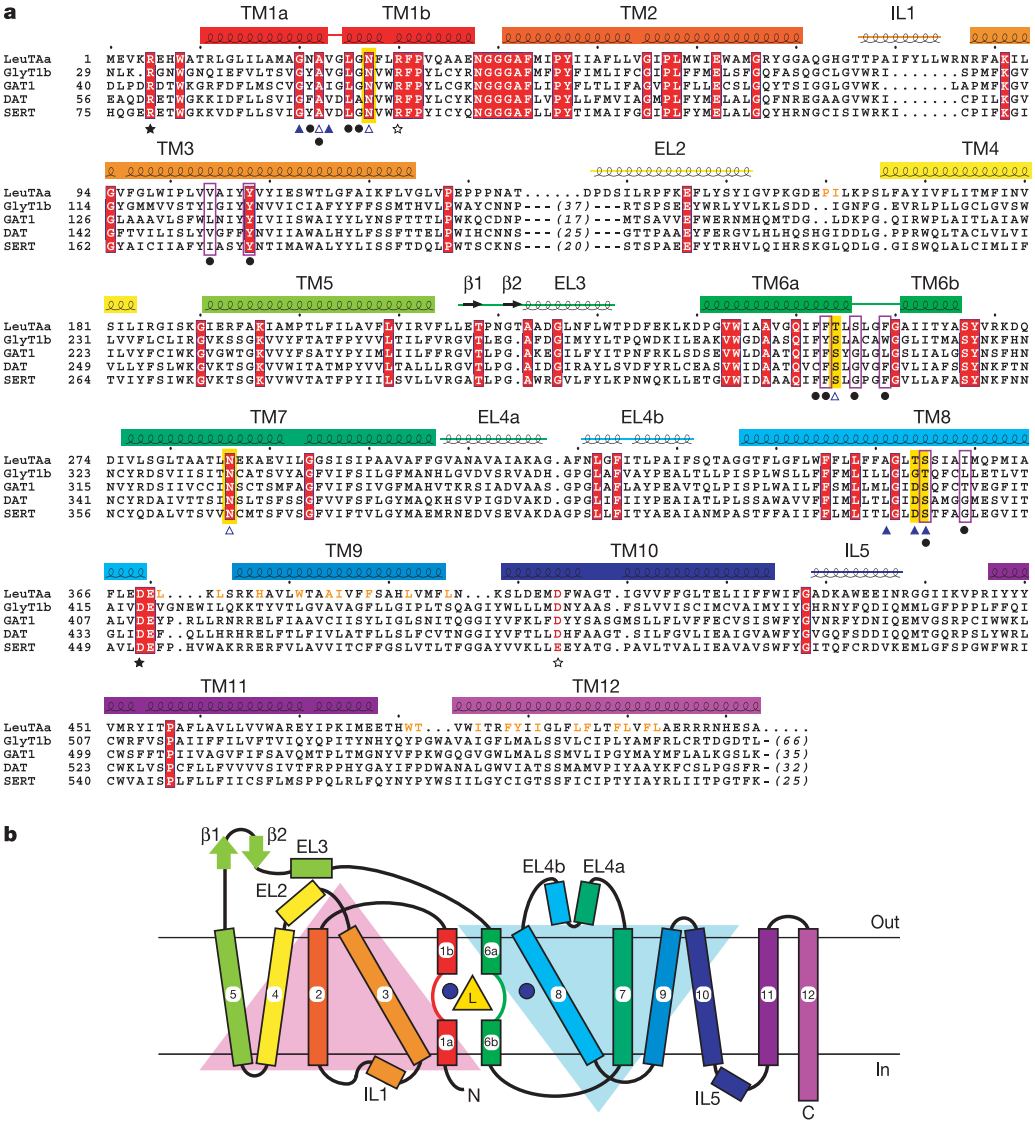

Figure 1 | Amino acid sequence alignment and secondary structure of $LeuT_{Aa}$. **a**, Amino acid sequence alignment of *A. aeolicus* $LeuT_{Aa}$ (NP_214423) with the human transporter homologues for glycine (GlyT1b; I57956), GABA (GAT1; P30531), dopamine (DAT; Q01959) and serotonin (SERT; P31645) using Psi-BLAST (http://www.ncbi.nlm.nih.gov/BLAST/) with manual adjustment. Strictly conserved residues are highlighted in red, and α-helices and β-strands in $LeuT_{Aa}$ are depicted as coils and arrows, respectively. The open and filled blue triangles show residues involved in coordinating sodium ions Na1 and Na2, respectively, and the residues whose side-chain atoms interact with the sodium ions are further highlighted in yellow. The filled black circles indicate the residues involved in L-leucine binding, and the residues whose side chains interact with the leucine are enclosed by purple boxes. The open and filled stars indicate the charged pairs at the extracellular and cytoplasmic entrances, respectively. The residues in the $LeuT_{Aa}$ dimer interface are shown in orange letters. For the eukaryotic transporters, residues at the N- and C termini and between TM3 and TM4 are truncated in the alignment, and the numbers of truncated residues are shown in parentheses. **b**, The $LeuT_{Aa}$ topology. The positions of leucine and the two sodium ions are depicted as a yellow triangle and blue circles, respectively.

Table 1 | **Refinement statistics**

Resolution (Å)	50–1.65
R_{work}/R_{free}*	0.199/0.217
Number of atoms	
Protein	4,044
Substrate/ion	12
Detergent	100
Water	210
B-factors	
Protein	27.7
Substrate/ion	19.2
Detergent	58.8
Water	44.2
R.m.s.d.	
Bond lengths (Å)	0.005
Bond angles (°)	1.111

*$R_{work} = \Sigma||F_o| - |F_c||/\Sigma|F_o|$. R_{free} is the *R*-value for a subset of 5% of the reflection data, which were not included in the crystallographic refinement.

pseudo repeats with opposite orientations in the membrane bilayer. Not surprisingly, there are bacterial homologues that possess only the first 10–11 transmembrane helices[18], thus reinforcing the concept that the first ten helices form the essential core of Na^+/Cl^--dependent neurotransmitter transporters. Interestingly, other membrane transport proteins, such as aquaporin[20] and the oxalate transporter[21], possess pseudo-two-fold axes parallel and perpendicular to the membrane.

TM1 and TM6, which harbour the greatest density of conserved residues (Fig. 1a), are oriented antiparallel to one another and, most importantly, are not continuous helices. In fact, TM1 and TM6 have breaks in helical structure at positions approximately halfway across the membrane bilayer. In TM1, residues Val 23 and Gly 24 adopt an extended conformation, linking segments 1a and 1b. The interruption of helical structure is greater in TM6, with residues Ser 256 to Gly 260 adopting extended, non-helical conformations. These two breaks in helical structure expose main-chain carbonyl oxygen and nitrogen atoms for hydrogen bonding and ion coordination. TM3 and TM8, long helices tilted by ~50° from the membrane normal, are also related by the pseudo-two-fold axis and possess key conserved amino acid residues located near the unwound segments of TM1 and TM6. As discussed below, TM3, TM8 and the zone surrounding the TM1 and TM6 unwound regions comprise the substrate and sodium ion binding sites.

The remaining transmembrane segments surround TM1, TM3, TM6 and TM8, support the protein core and comprise most of the lipid-exposed $LeuT_{Aa}$ surface, with TM2 and TM7 buttressing TM6 and TM1, respectively. A prominent V-shaped structure formed by TM4–TM5 and a pseudo-two-fold related inverted V created by TM9–TM10 hold TM3 and TM8 like pincers. TM10 is followed by TM11 and TM12, flanking the outer surfaces of TM9 and TM10. TM12 is a helix to the C terminus of the protein and protrudes the deepest into the cytoplasm (Fig. 2a). Conserved amino acid residues are observed throughout TM2, TM4, TM5, TM7 and TM9–TM12 (Fig. 1a), reinforcing their importance in structure and function.

There are substantial helical and loop segments on the solvent-exposed surfaces of $LeuT_{Aa}$, some of which are situated in regions that suggest a role in the transport mechanism. The first six residues at the N terminus (Arg 5 to Thr 10) possess an extended structure and are located in the crevices between the ends of TM1a, TM4, TM5, TM6b and TM8 (Supplementary Fig. 1). Specifically, two strictly conserved residues, Arg 5 and Trp 8, make numerous interactions in these crevices. Between TM2 and TM3 are a re-entrant segment of polypeptide and a short helix (IL1) that occlude the intracellular face of $LeuT_{Aa}$ (Supplementary Fig. 1). On the opposite side of the bilayer, between TM3 and TM4, a stretch of 41 residues (EL2) reaches 'up' from TM3 via extended polypeptide and then returns 'down' to TM4 via a helix and a β-turn. In eukaryotic transporters the number of residues between TM3 and TM4 is substantially greater (Fig. 1a), harbouring glycosylation sites[9] and a probable disulphide bond[22,23].

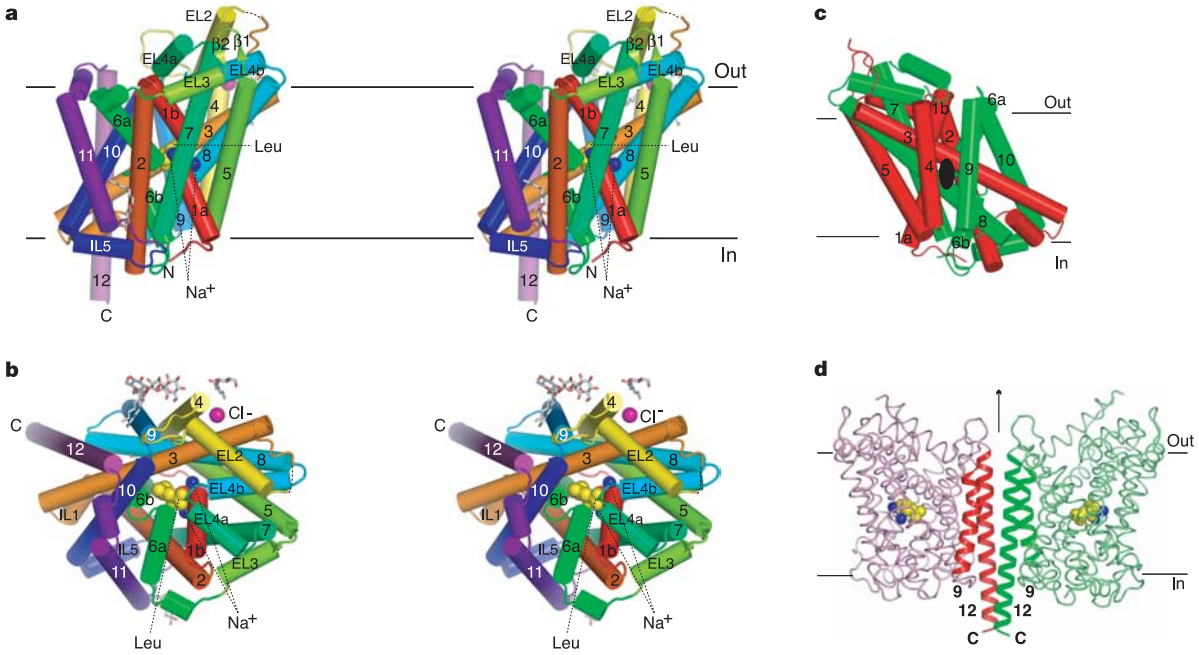

Figure 2 | **$LeuT_{Aa}$ structure.** **a**, Stereoview in the plane of the membrane. Bound L-leucine, two sodium ions and a chloride ion are shown as CPK models in yellow, blue and magenta, respectively. Detergent molecules (β-OG) are shown as stick models. Colouring and numbering of helices (cylinders) and strands (arrows) are the same as in Fig. 1. **b**, Stereoview from the extracellular side. **c**, Pseudo-symmetry in the $LeuT_{Aa}$ molecule. Shown are transmembrane segments TM1–TM10, viewed approximately parallel to the pseudo-two-fold axis of symmetry that relates TM1–TM5 (red) and TM6–TM10 (green). The pseudo-two-fold rotation axis is depicted as a black ellipsoid. **d**, The $LeuT_{Aa}$ dimer, with the subunits related by the crystallographic two-fold axis of symmetry (black arrow). One protomer is light green, the other is pink, and TM9 and TM12 are highlighted and numbered. Leucine and the sodium ions are shown in CPK representation in yellow and blue, respectively.

The helical segment of EL2 is juxtaposed across from EL4, a segment of polypeptide between TM7 and TM8 that is composed of two short helices separated by an acute bend. The EL4a helix, in turn, makes numerous contacts with TM1b. Together, EL2 and EL4 define a portion of the shot-glass rim above the membrane bilayer.

$LeuT_{Aa}$ forms a dimer in the crystal, located on the two-fold axis of crystallographic symmetry, and the two protomers adopt a parallel orientation (Fig. 2d). The dimer interface is formed by EL2, TM9 and TM12, and the latter two elements of structure, together with their symmetry partners, form a four-helix bundle (Fig. 1a; see also Supplementary Fig. 2). The relevance of this interface to eukaryotic NSS members, most of which are thought to form oligomers, is supported by experiments on SERT, which indicate that TM12, together with TM11, participate in multimerization[24]. TM2, TM4 and TM6 have also been implicated in dimerization of some eukaryotic counterparts[25], but because TM2 and TM6 are substantially sequestered within the $LeuT_{Aa}$ core, it is unlikely that these transmembrane segments participate in extensive protomer–protomer contacts in eukaryotic transporters. However, TM4, which lies on the surface, could partake in multimerization, although it is not part of the $LeuT_{Aa}$ dimer interface.

Leucine binding site

Prominent non-protein electron density located in the core of the $LeuT_{Aa}$ protein, near the middle regions of TM3 and TM8 and adjacent to the unwound regions of TM1 and TM6 (Fig. 3a), pin-pointed the location of substrate and sodium ion binding sites. The larger electron density feature indicated that it was L-leucine, whereas the other two were interpreted as sodium ions (see below). Indeed, $LeuT_{Aa}$ reconstituted into liposomes exhibited sodium-dependent uptake of L-leucine (Fig. 3b). Transport was not chloride dependent, consistent with the absence of a chloride ion located near the leucine and sodium ions, although a chloride ion is bound on the outer surface of the protein (Fig. 2a, b; see also Supplementary Fig. 3). Leucine uptake by $LeuT_{Aa}$ proteoliposomes was stimulated ~20–30% by valinomycin, suggesting that under the current assay conditions leucine transport is enhanced by vesicles with an internal negative potential, and therefore transport may be electrogenic (Supplementary Fig. 4a). Further experiments, however, are required to establish the stoichiometries of substrate and ion(s) in the transport cycle of $LeuT_{Aa}$.

The most striking feature of the leucine binding site is that exposed main chain atoms from the unwound regions of TM1 and TM6 make most of the contacts with the α-amino and α-carboxy groups of the bound leucine (Fig. 3c). Unwinding of TM1 and TM6 not only affords direct hydrogen-bonding partners but also allows the α-amino and α-carboxy groups to bind close to the ends of the helical segments and exploit α-helix dipole moments. Specifically, the negatively charged ends of the TM1a and TM6a helix dipoles are proximal to the amino group of leucine, whereas the positively charged end of the TM1b helix dipole is near the carboxy group. Notably, no residues that bear a formal charge interact with the α

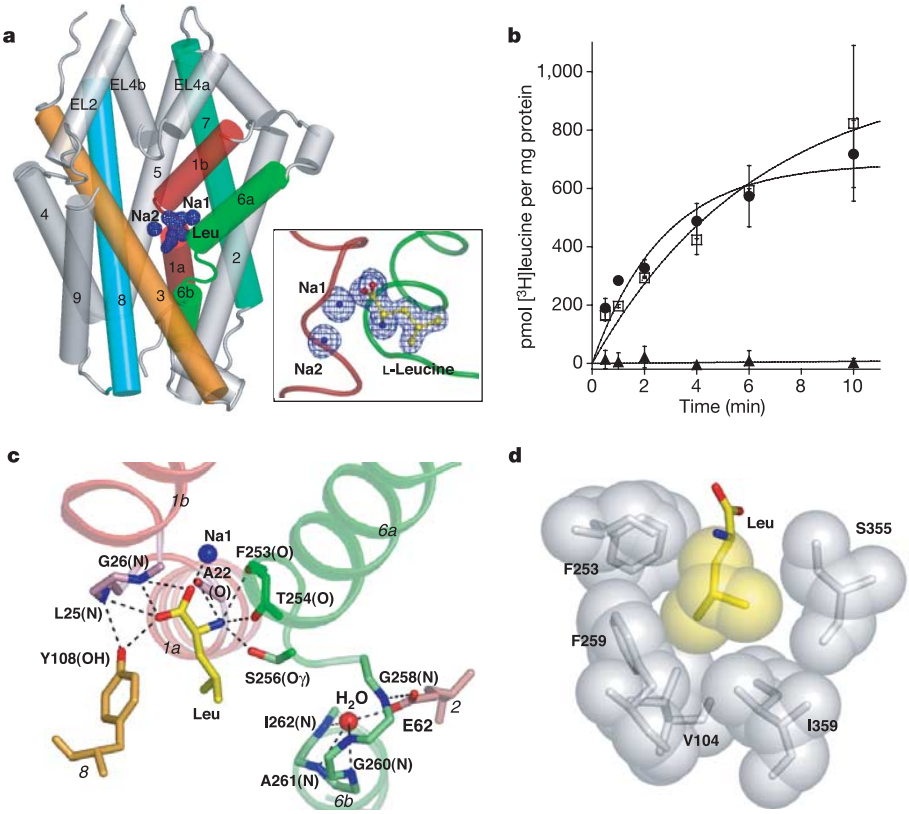

Figure 3 | Leucine binding site. **a**, $F_o - F_c$ simulated-annealing omit map, contoured at 3.8σ, showing density for leucine and sodium ions, where leucine and the two sodium ions were omitted from the simulated annealing run and subsequent phase calculation. View of $LeuT_{Aa}$ rotated 110° anticlockwise in the membrane plane and 25° towards the reader relative to the view in Fig. 2a. TM10–TM12 are omitted from the figure for clarity. A magnified view of the density is shown in the enclosed box. **b**, [^{3}H]Leucine transport by $LeuT_{Aa}$ reconstituted into liposomes. The filled circles, open squares and filled triangles represent uptake from an external solution containing NaCl (sodium and chloride gradients), sodium gluconate (sodium gradient) and KCl (chloride gradient), respectively. The data points were fit to a single exponential (solid line). Error bars for each data point represent the standard deviation for duplicate measurements. **c**, Hydrogen bonds and ionic interactions in the leucine binding pocket are depicted as dashed lines. **d**, Hydrophobic interactions between the leucine and $LeuT_{Aa}$. Van der Waals surfaces for the leucine side chain and interacting residues are shown as spheres. Tyr 108 and Ser 256 are omitted from the figure for clarity.

substituents of leucine. Furthermore, the leucine binding site is completely dehydrated, and the closest water molecules are >9 Å away from the leucine α-carbon atom (Supplementary Fig. 5). Although we cannot directly discern the ionization state of the α substitutents from our electron density maps, the pattern of hydrogen bonding interactions suggests that leucine is bound as a zwitterion.

Copious polar contacts, therefore, satisfy the hydrogen bonding requirements of the charged α substituents. The amino group is coordinated by main-chain carbonyl oxygens from Ala 22 in TM1, Phe 253 and Thr 254 in TM6, and by a side-chain hydroxyl from Ser 256 in TM6. The carboxy group interacts with a sodium ion, amide nitrogens from Leu 25 and Gly 26 in TM1, and a hydroxyl from Tyr 108 in TM3 (Fig. 3c). The Tyr 108 hydroxyl also forms a hydrogen bond with the main-chain amide nitrogen of Leu 25, an interaction that may function as a latch to stabilize the irregular structure near the unwound region in TM1 (Fig. 3c). This tyrosine is strictly conserved among all NSS family members (Fig. 1a) and has been implicated in substrate binding and transport in GAT1 (ref. 12), SERT[13] and GLYT2a[26]. The structure of the unwound region in TM6 is stabilized by Glu 62, which interacts with the amide nitrogen of Gly 258 directly and with the amide nitrogens of Gly 260, Ala 261 and Ile 262 through a water molecule (Fig. 3c). This glutamate is conserved (Fig. 1a) and in GAT1 its replacement by aspartate renders the transporter inactive[27].

The aliphatic side chain of leucine, by contrast with the α substituents, is cradled within a hydrophobic pocket created by the side-chain atoms of Val 104 and Tyr 108 in TM3, Phe 253, Ser 256 and Phe 259 in TM6, and Ser 355 and Ile 359 in TM8. The complementarity of the van der Waals surface formed by these residues to the side chain of L-leucine (Fig. 3d) is consistent with the specificity of $LeuT_{Aa}$ for its namesake substrate. Indeed, in a competition experiment 0.1 mM cold L-leucine quantitatively blocks uptake, whereas 0.1 mM of either glycine or tryptophan are much less effective competitors, reducing the uptake of [^{3}H]leucine by only ~30% (Supplementary Fig. 4b).

The location of the substrate binding site in $LeuT_{Aa}$, together with amino acid sequence information on eukaryotic homologues, allows us to understand why some eukaryotic transporters are specific for glycine and GABA, molecules that possess amino and carboxy groups, whereas other transporters are specific for biogenic amines, including dopamine, serotonin and norepinephrine, molecules that lack a carboxy group. Amino acid sequence analysis illustrates that a key difference between amino acid and biogenic amine transporters is that the former have a glycine and the latter have an aspartate at position 24 in the $LeuT_{Aa}$ sequence[10] (Fig. 1a). Upon modelling an aspartate at glycine 24, we can position the β-carboxy group of the aspartate to within 1 Å of the carboxy group of the substrate leucine and within 3 Å of a sodium ion. Therefore, we propose that in the biogenic amine transporters the aspartate's carboxy group supplants the carboxy group of amino acid substrates and coordinates a sodium ion. In addition, the carboxy group of the aspartate in the biogenic amine transporters may form a hydrogen bond to the amine group of the substrate and the hydroxyl group of Tyr 108.

Identification of residues shaping the leucine binding site in $LeuT_{Aa}$ illuminates determinants of substrate specificity in the eukaryotic homologues. In the glycine transporter GlyT1b, for example, residues at equivalent positions to those surrounding the isopropyl moiety of leucine in $LeuT_{Aa}$ are replaced with amino acids of a larger size or different shape, such as Val 104 to Ile, Phe 259 to Trp and Ile 359 to Leu (Fig. 1a). Together, these changes reduce the volume of the binding pocket, thereby rendering it more complementary to glycine. By contrast, residues in SERT are replaced with smaller amino acids, such as Ser 256 to Gly and Ile 359 to Gly (Fig. 1a), to accommodate the larger serotonin molecule. Phe 259, also a phenylalanine in the biogenic amine transporters (Fig. 1a), may participate in π–π stacking interactions with the aromatic rings of serotonin, dopamine or norepinephrine in their respective transporters.

Sodium binding sites

In the $LeuT_{Aa}$ structure we have identified two sodium ion binding sites, named Na1 and Na2, within 6 Å of the α-carbon of the bound leucine molecule, located halfway across the membrane bilayer, at the unwound regions of TM1 and TM6 (Fig. 3a). Because distinguishing between a sodium ion and a water molecule, even at 1.65 Å resolution, is non-trivial, we based our determination on a number of observations. First, when the two peaks were modelled as oxygen atoms of water molecules there was residual density greater than 3σ in electron density maps calculated with $F_o - F_c$ coefficients, after refinement of atomic positions and temperature factors, even though the temperature factors of the oxygen atoms refined to values that were lower (10.41 and 8.81 Å^2) than those of surrounding protein atoms. Second, when the two electron density features were modelled as sodium ions, the $F_o - F_c$ residual density disappeared, and the temperature factors refined to values (17.28 and 15.78 Å^2) comparable to those of neighbouring protein atoms. Third, valence calculations[28] yielded a sodium-specific valence (ν_{Na^+}) of 1.32 for Na1 and 1.34 for Na2, in agreement with the values expected for bound sodium ions ($\nu_{Na^+} \geq 1.0$). By contrast, Li^+, K^+ and Mg^{2+} yielded valence values far from the expected figures. Fourth, the distances between the sodium ions and coordinating atoms were appropriate for sodium but too short for water or potassium. Valence calculations on all the other water molecules built into the electron density did not suggest the presence of additional cations.

The two sodium ions have key roles in stabilizing the $LeuT_{Aa}$ core, the unwound structures of TM1 and TM6, and the bound leucine molecule. Octahedral coordination of Na1 is provided by the leucine carboxy oxygen, the carbonyl oxygens of Ala 22 (TM1) and Thr 254 (TM6), the side-chain carbonyl oxygens of Asn 27 (TM1) and Asn 286 (TM7), and the hydroxyl oxygen of Thr 254 (TM6; Fig. 4a). In the biogenic amine transporters, an aspartate residue, located at position 24 in the $LeuT_{Aa}$ sequence, probably coordinates a sodium ion equivalent to Na1. Na2 is positioned between the TM1 unwound region and TM8, about 7.0 Å from Na1 and 5.9 Å from the α-carbon of bound leucine (Fig. 3a). Trigonal bi-pyramidal coordination to Na2 is achieved by carbonyl oxygens from Gly 20 and Val 23 (TM1), Ala 351 (TM8), and the hydroxyl oxygens from Thr 354 and Ser 355 (TM8; Fig. 4b). Notably, coordination for both Na1 and Na2 is accomplished by partial charges from the protein, with the carboxy group of the bound leucine being the only ligand bearing a formal charge.

What do the sodium binding sites in the $LeuT_{Aa}$ structure tell us about the mechanism by which Na^+/Cl^--dependent transporters preferentially bind sodium instead of potassium, ions that differ in ionic radius by only ~0.38 Å? We suggest that the primary mechanism is that the sodium binding sites in $LeuT_{Aa}$ are simply too 'small' to accommodate the larger potassium ion. Indeed, the mean sodium ion–ligand distance in $LeuT_{Aa}$ is 2.28 Å (σ = 0.15 Å), a distance that agrees well with sodium ion–oxygen distances obtained from high-resolution crystal structures[29]. By comparison, the mean potassium–oxygen distances are 2.84 Å[29]. The ion binding sites in $LeuT_{Aa}$ are devoid of water (Supplementary Fig. 5) and in order for the protein to compensate for the unfavourable dehydration of sodium ions, it must form precise binding sites complementary in size and charge. Because the sodium ions are situated within the core of the protein, the binding sites are constrained from expanding or contracting by a large number of hydrogen-bonding and packing interactions, and are unable to accommodate ions of different size or valence. In fact, the residues surrounding the sodium and leucine binding sites are the most well defined in the entire structure, as indicated by low crystallographic temperature factors (data not shown).

The intimate disposition of the sodium and leucine binding sites implies a mechanism for the coupling of sodium and substrate

transport. We suggest that binding of sodium ions is required to organize the substrate binding site, which is partially formed by the potentially flexible and unwound regions of TM1 and TM6, for high-affinity substrate binding. The coordination of the two sodium ions by residues in TM7 and TM8 further stabilizes the architecture of the substrate-binding site (Fig. 4).

The $LeuT_{Aa}$ structure, together with functional and amino acid sequence data on eukaryotic homologues, suggest that the Na1 site is present in eukaryotic NSS family members. First, TM1, TM6 and TM7, the helices surrounding Na1, are implicated in sodium binding in GAT1 (ref. 30), SERT[31] and DAT[32]. Second, coordinating residues are conserved or conservatively substituted in NSS transporters (Fig. 1a), and in SERT the residue equivalent to Asn 286 is involved in sodium binding[31]. In an invertebrate NSS homologue that can use either Na^+ or K^+ to drive uptake of neutral amino acids, the corresponding residue is an aspartate, and mutation of this residue alters ion selectivity[33], suggesting that this transporter also shares the Na1 site. Residues coordinating Na2, by contrast, are less well conserved. For example, Thr 354 is a glycine in GlyT1b and an aspartate in GAT1 and the biogenic amine transporters (Fig. 1a). Whereas the aspartate residue probably participates in sodium coordination, in GlyT1b the loss of the threonine hydroxyl leaves only four coordinating atoms and begs the question of whether this site is present in GlyT1b.

Sodium ion to substrate stoichiometry required for transport varies among eukaryotic transporters and is certainly related to the number of sodium ion binding sites. Although the norepinephrine transporter (NET)[15] and SERT[15] both transport Na^+ and their respective substrate in a ratio of 1:1 (ref. 15), the sodium-to-substrate ratio in GAT1 (ref. 16) and GlyT1b[17] is 2:1, and in GlyT2a it is 3:1 (ref. 17). We suggest that the Na1 site is a common binding site for the co-transported sodium ion in all NSS members and that those transporters with 2:1 and 3:1 stoichiometries have additional sites that may include the Na2 site. At present, the location of a third sodium site is unknown.

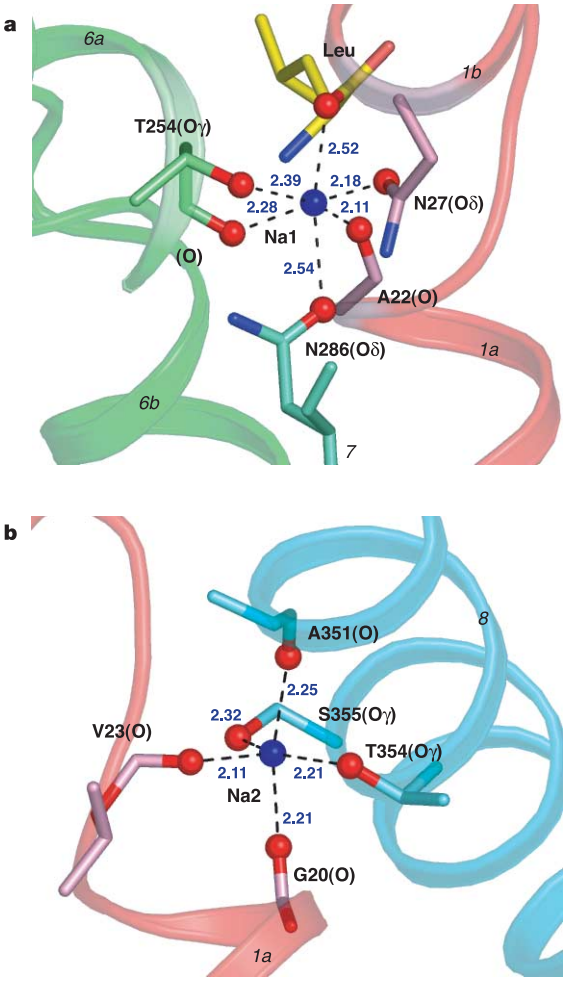

Figure 4 | Sodium ion binding sites. a, Na1 and residues from TM1a, TM1b, TM6a and TM7 together with bound leucine are shown. **b**, Na2 and residues from TM1a and TM8 are shown. Distances (Å) are in blue letters.

Mechanistic implications

Na^+/Cl^--dependent transporters are membrane-spanning proteins that catalyse the movement of molecules (substrates) and ions across lipid bilayer membranes. These transporters, like many ion channels, have selective binding sites for permeant molecules and ions, but unlike most ion channels, transporters are believed to possess two 'gates' that can alternately allow access to the binding sites from either side of the membrane bilayer, as judged by their function[34]. The $LeuT_{Aa}$ crystal structure defines the residues and protein domains that comprise the extracellular and intracellular gates, and it suggests conformational changes that might occur during the transport cycle.

The conformation of the $LeuT_{Aa}$ protein reported here is one in which the leucine and sodium sites are occluded from solution on both the extracellular and cytoplasmic sides of the protein; that is, both the extracellular and intracellular gates are closed. Access to the extracellular solution from the leucine and sodium binding sites is primarily obstructed by Tyr 108 and Phe 253, and layered on top of these aromatic residues is a conserved charged pair composed of Arg 30 and Asp 404, which together define at least part of the extracellular gate (Fig. 5a). Arg 30 and Asp 404 interact via a pair of water molecules but could form a salt bridge upon rearrangement of the guanidium group (Fig. 5b). Arg 30 also forms a cation–π interaction with Phe 253, and is ultimately connected to Na1 via a hydrogen-bond network that includes Gln 250. These residues are highly conserved in the NSS family (Fig. 1a), with residues equivalent to Arg 30 and Asp 404 being important for eukaryotic transporter function[14,35]. The charged pair lies at the bottom of the extracellular cavity, lined with small pockets and protrusions, defined by TM1b, TM3, TM6a, TM8, TM10 and the 'V-shaped' tip of EL4 (Figs 3a and 5a). We suggest that when the extracellular gate is open, Arg 30 and Asp 404 may move apart, disrupting their interaction. When the gate is closed, Arg 30 and Asp 404 form a water-mediated salt link, stabilizing the extracellular gate in a closed conformation.

In contrast to the extracellular gate, where just a few residues obstruct the leucine and sodium ion binding sites, the cytoplasmic gate is far more substantial, being composed of ~20 Å of ordered protein structure (Fig. 5a). Directly beneath the leucine and sodium binding sites are TM1a, TM6b and TM8, with these main-chain scaffolds themselves blocking cytoplasmic access to the binding sites. Near the cytoplasmic face of the protein, another conserved charged pair, Arg 5 and Asp 369, forms an important and partially buried salt bridge. Arg 5 also forms a hydrogen bond with Ser 267 and a cation–π interaction with Tyr 268 (Fig. 5c). Adjacent to these residues lies Trp 8, the indole ring of which fits snugly in a hydrophobic pocket created by TM1a and TM6b, with its Nε nitrogen atom hydrogen bonding to the carbonyl oxygen of Tyr 265 in TM6b (Fig. 5c). The conserved Trp 8 stabilizes the conformation of TM1a–TM6b and anchors the amino terminus, including Arg 5. All these residues are strictly conserved among other NSS family members (Fig. 1a), and mutation of residues equivalent to either Arg 5 or Trp 8 in GAT1 (ref. 36) and Asp 369 (ref. 37) or Tyr 268 (ref. 38) in DAT impairs transport.

How might the extracellular and cytoplasmic gates open? The architecture of $LeuT_{Aa}$ provides tantalizing clues to possible movements of the protein backbone. If we consider the unwound regions as 'joints', we suggest that the extracellular and cytoplasmic helical segments, that is TM1b–TM6a and TM1a–TM6b, respectively, might

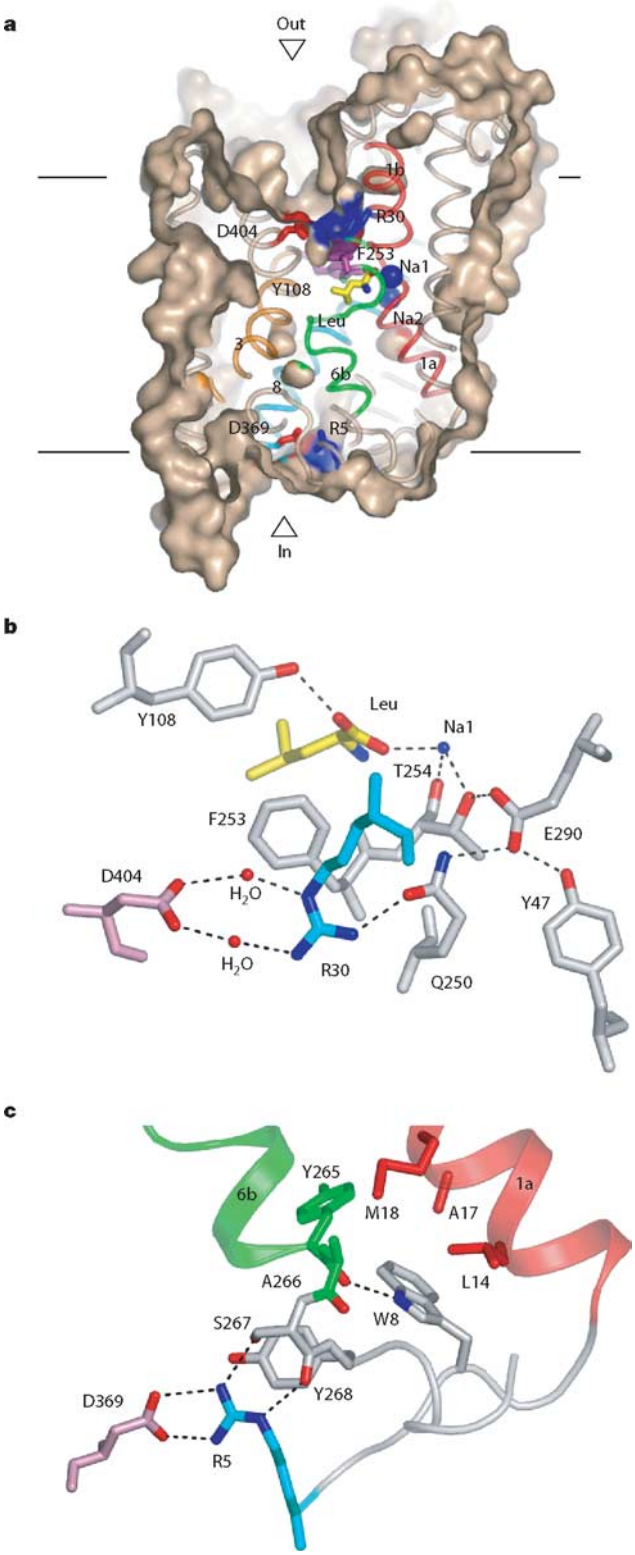

Figure 5 | **Extracellular and cytoplasmic gates. a**, Slice through the surface of $LeuT_{Aa}$, viewed parallel to the membrane, showing the extracellular cavity. Connolly surface of $LeuT_{Aa}$ is shown in beige. L-Leucine, Tyr 108, Phe 253 and the two charged pairs (Arg 30–Asp 404 and Arg 5–Asp 369) are depicted as stick models in yellow for leucine, purple for aromatic residues, blue for arginines and red for aspartates. **b**, **c**, Key interacting residues at the extracellular (**b**) and at the cytoplasmic (**c**) gate.

move relative to TM3 and TM8, helping to open and close the outward and inward gates (Fig. 6). Binding and unbinding of substrate and ions to the unwound joints may stabilize the helices in different conformational states. In calcium ATPase, for example, binding and release of calcium ions to unwound regions in transmembrane helices effects structural rearrangements[39]. Movement in TM1 may be accompanied by a conformational change in the linker between TM1 and TM2, which contains the highly conserved motif NGGGAF. In GLYT2a[40] and SERT[41], accessibility studies have revealed that this region moves during the transport cycle. We suggest that TM3 and TM8 may also shift their positions or rotate slightly. In addition, the extracellular and cytoplasmic entries could expand upon movement of surface-exposed elements, including the N terminus, IL1, EL2 and EL4. Indeed, construction of chimaeras between NET and SERT revealed that both EL2 (ref. 42) and EL4 (ref. 43) participate in conformational changes during transport. Finally, the surrounding transmembrane segments, TM2, TM7, TM10 and TM11, may accommodate movement of TM1, TM3, TM6 and TM8 because they have interruptions in the middle of their helical structures caused by Gly 55 and Pro 57 in TM2, Gly 294 in TM7, Gly 408 in TM10 and Pro 457 in TM11, most of which are conserved residues in the NSS family (Fig. 1a).

Discussion

The structure of $LeuT_{Aa}$, together with that of the prokaryotic glutamate transporter homologue Glt_{Ph} of *Pyrococcus horikoshii*[44], a representative of the other family of plasma membrane neurotransmitter transporters, reveals important common principles between them, although their overall folds are markedly different. First, both structures have captured an occluded state, therefore suggesting that mechanisms of transport for these transporters must include at least three iconic states: open to outside, occluded, and open to inside. Second, key portions of the substrate and ion binding sites are composed of extended elements of polypeptide insinuated in the middle of disrupted transmembrane α-helices, thereby allowing main-chain atoms to participate in hydrogen bonding interactions. Finally, substrate and sodium binding sites ($LeuT_{Aa}$) or residues implicated in sodium binding (Glt_{Ph}) are located close in three-dimensional space, thereby demonstrating that the long-described thermodynamic coupling of substrate and ion transport in these two families of sodium-dependent transporters is the consequence of direct or nearly direct interactions.

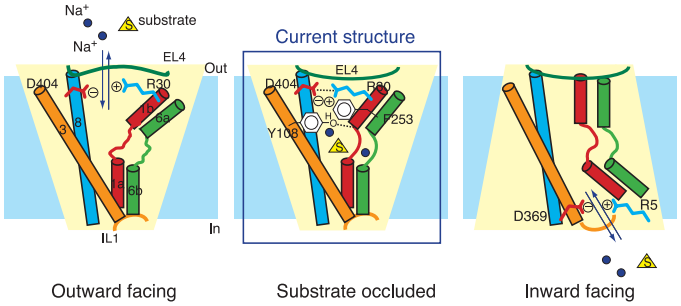

Figure 6 | **Speculative transport mechanism.** Schematic drawing of a possible conformational change upon substrate/sodium ion transport. The left panel shows the outward-facing state. TM1a and TM6b assume the closed arrangement, whereas TM1b and TM6a adopt the open one. The middle panel shows the substrate-occluded state, which corresponds to the current crystal structure. TM1a and TM6b assume the closed arrangement, whereas TM1b and TM6a adopt a partially open one with some residues blocking the permeation pathway. The right panel shows the inward-facing state. TM1b and TM6a assume the closed arrangement, whereas TM1a and TM6b adopt the closed one, to open the pathway to the cytoplasm.

METHODS

Crystallization. The DNA coding for *A. aeolicus* $LeuT_{Aa}$ was amplified by polymerase chain reaction from genomic DNA and cloned into a pET16b derivative that included a C-terminal octahistidine tag and a thrombin site. The protein was produced in *Escherichia coli* C41 cells cultured in Terrific broth after induction at an absorbance at 600 nm (A_{600}) of 0.6 with 0.1 mM isopropyl-β-D-thiogalactopyranoside for 20 h at 20 °C. Cell membranes were isolated from disrupted cells and solubilized with 40 mM dodecylmaltoside (DDM). $LeuT_{Aa}$ was eluted from a metal ion affinity chromatography column in buffer composed of 20 mM Tris-HCl (pH 8.0), 190 mM NaCl, 10 mM KCl, 300 mM imidazole and 1 mM DDM. After thrombin digestion, the protein was loaded onto a size exclusion column equilibrated in 20 mM Tris-HCl (pH 8.0), 190 mM NaCl, 10 mM KCl, and 40 mM *n*-octyl-β-D-glucopyranoside (β-OG). Purified protein was concentrated and dialysed overnight at 4 °C against 10 mM Tris-HCl (pH 8.0), 45 mM NaCl, 5 mM KCl and 40 mM β-OG before crystallization. Selenomethionine-labelled protein (SeMet-$LeuT_{Aa}$) was expressed in C41 cells as previously reported[45], using 1 mM β-mercaptoethanol in all buffers to minimize oxidation.

$LeuT_{Aa}$ crystals were grown by hanging-drop vapour diffusion at 18 °C by mixing protein solution ($\sim 7\ mg\ ml^{-1}$) with a reservoir solution composed of 0.1 M HEPES-NaOH (pH 7.0), 18–22% PEG 550 MME, and 0.2 M NaCl. Before freezing in liquid nitrogen, crystals were cryoprotected with a reservoir solution containing 35% PEG 550 MME and 40 mM β-OG. The crystals belong to the space group of *C*2 with cell dimensions of $a = 87.9$ Å, $b = 86.3$ Å, $c = 81.0$ Å and $\beta = 95.7°$.

Structure determination. X-ray diffraction data sets were collected using an ADSC QUANTUM 315 detector at the Advanced Light Source 8.2.2 and processed with HKL2000. Phases were obtained by the multiwavelength anomalous dispersion method[19] using a three-wavelength data set from a SeMet-$LeuT_{Aa}$ crystal. The program SOLVE[46] was used to determine selenium sites and initial phases, which were improved by solvent flattening and histogram matching using DM[47]. The initial structure was automatically built by Arp/wArp[48], subsequent manual rebuilding was accomplished with TURBO-FRODO, and the model was refined with CNS[49].

Transport assay. Proteoliposomes were reconstituted as described previously[50] using $LeuT_{Aa}$ as purified for crystallization except with 1 mM DDM as the detergent. L-Leucine uptake was initiated by diluting liposomes loaded with buffer 1 (20 mM HEPES-Tris, pH 7.4, 100 mM potassium gluconate) supplemented with 1 μM valinomycin into a 200-fold excess of buffer 2 (20 mM HEPES-Tris, pH 7.4, 0.1 μM L-[3,4,5-^{3}H(N)]leucine) also containing 1 μM valinomycin and either 100 mM NaCl, 100 mM sodium gluconate, or 100 mM KCl at 20 °C. Reactions were quenched by diluting each assay tenfold with ice-cold buffer 1, followed by filtration through nitrocellulose filters. The filters were washed twice with 1 ml of ice-cold buffer 1, placed in scintillation fluid, and counted on a scintillation counter. Background counts were subtracted from each data point and were estimated by averaging [^{3}H]leucine counts over a 10-min time window using liposomes prepared in the absence of $LeuT_{Aa}$ and reaction conditions as described above. Specific transport activity was estimated from the protein concentration before reconstitution, assuming an incorporation efficiency of 100%. The experiments probing valinomycin dependence and substrate competition are described in Supplementary Information.

Received 23 May; accepted 4 July 2005.
Published online 24 July 2005.

1. Vanhatalo, S. & Soinila, S. The concept of chemical neurotransmission — variations on the theme. *Ann. Med.* **19,** 151–158 (1998).
2. Masson, J., Sagne, C., Hamon, M. & Mestikawy, S. E. Neurotransmitter transporters in the central nervous system. *Pharm. Rev.* **51,** 439–464 (1999).
3. Hahn, M. K. & Blakely, R. D. Monoamine transporter gene structure and polymorphisms in relation to psychiatric and other complex disorders. *Pharmacogenomics J.* **2,** 217–235 (2002).
4. Richerson, G. B. & Wu, Y. Role of the GABA transporter in epilepsy. *Adv. Exp. Med. Biol.* **548,** 76–91 (2004).
5. Amara, S. G. & Sonders, M. S. Neurotransmitter transporters as molecular targets for addictive drugs. *Drug Alcohol Depend.* **51,** 87–96 (1998).
6. Krogsgaard-Larsen, P., Frolund, B. & Frydenvang, K. GABA uptake inhibitors. Design, molecular pharmacology and therapeutic aspects. *Curr. Pharm. Des.* **6,** 1193–1209 (2000).
7. Barker, E. L. & Blakely, R. D. in *Psychopharmacology—the Fourth Generation of Progress* (eds Bloom, F. E. & Kupfer, D. J.) (Raven Press, New York, 2000).
8. Guastella, J. *et al.* Cloning and expression of a rat brain GABA transporter. *Science* **249,** 1303–1306 (1990).
9. Nelson, N. The family of Na^+/Cl^--dependent neurotransmitter transporters. *J. Neurochem.* **71,** 1785–1803 (1998).
10. Torres, G. E., Gainetdinov, R. R. & Caron, M. G. Plasma membrane monoamine transporters: structure, regulation, and function. *Nature Rev. Neurosci.* **4,** 13–25 (2003).
11. Chen, J. G., Liu-Chen, S. & Rudnick, G. Determination of external loop topology in the serotonin transporter by site-directed chemical labeling. *J. Biol. Chem.* **273,** 12675–12681 (1998).
12. Bismuth, Y., Kavanaugh, M. P. & Kanner, B. I. Tyrosine 140 of the γ-aminobutyric acid transporter GAT-1 plays a critical role in neurotransmitter recognition. *J. Biol. Chem.* **272,** 16096–16102 (1997).
13. Chen, J. G., Sachpatzidis, A. & Rudnick, G. The third transmembrane domain of the serotonin transporter contains residues associated with substrate and cocaine binding. *J. Biol. Chem.* **272,** 28321–28327 (1997).
14. Cao, Y., Li, M., Mager, S. & Lester, H. A. Amino acid residues that control pH modulation of transport-associated current in mammalian serotonin transporters. *J. Neurosci.* **18,** 7739–7749 (1998).
15. Rudnick, G. in *Neurotransmitter Transporters: Structure, Function, and Regulation* (ed. Reith, E. A.) 25–52 (Humana Press, Totowa, New Jersey, 2002).
16. Kavanaugh, M. P., Arriza, J. L., North, R. A. & Amara, S. G. Electrogenic uptake of γ-aminobutyric acid by a cloned transporter expressed in *Xenopus* oocytes. *J. Biol. Chem.* **267,** 22007–22009 (1992).
17. Roux, M. & Supplisson, S. Neuronal and glial glycine transporters have different stoichiometries. *Neuron* **25,** 373–383 (2000).
18. Androutsellis-Theotokis, A. *et al.* Characterization of a functional bacterial homologue of sodium-dependent neurotransmitter transporters. *J. Biol. Chem.* **278,** 12703–12709 (2003).
19. Hendrickson, W. A. Determination of macromolecular structures from anomalous diffraction of synchrotron radiation. *Science* **254,** 51–58 (1991).
20. Murata, K. *et al.* Structural determinants of water permeation through aquaporin-1. *Nature* **407,** 599–605 (2000).
21. Hirai, T. *et al.* Three-dimensional structure of a bacterial oxalate transporter. *Nature Struct. Biol.* **9,** 597–600 (2002).
22. Chen, J. G., Liu-Chen, S. & Rudnick, G. External cysteine residues in the serotonin transporter. *Biochemistry* **36,** 1479–1486 (1997).
23. Wang, J. B., Moriwaki, A. & Uhl, G. R. Dopamine transporter cysteine mutants: second extracellular loop cysteines are required for transporter expression. *J. Neurochem.* **64,** 1416–1419 (1995).
24. Just, H., Sitte, H. H., Schmid, J. A., Freissmuth, M. & Kudlacek, O. Identification of an additional interaction domain in transmembrane domains 11 and 12 that supports oligomer formation in the human serotonin transporter. *J. Biol. Chem.* **279,** 6650–6657 (2004).
25. Sitte, H. H., Farhan, H. & Javitch, J. A. Sodium-dependent neurotransmitter transporters: oligomerization as a determinant of transporter function and trafficking. *Mol. Interv.* **4,** 38–47 (2004).
26. Ponce, J., Biton, B., Benavides, J., Avenet, P. & Aragon, C. Transmembrane domain III plays an important role in ion binding and permeation in the glycine transporter GLYT2. *J. Biol. Chem.* **275,** 13856–13862 (2000).
27. Keshet, G. I. *et al.* Glutamate-101 is critical for the function of the sodium and chloride-coupled GABA transporter GAT-1. *FEBS Lett.* **371,** 39–42 (1995).
28. Nayal, M. & Di Cera, E. Valence screening of water in protein crystals reveals potential Na^+ binding sites. *J. Mol. Biol.* **256,** 228–234 (1996).
29. Harding, M. M. Metal-ligand geometry relevant to proteins and in proteins: sodium and potassium. *Acta Crystallogr. D* **58,** 872–874 (2002).
30. Mager, S. *et al.* Ion binding and permeation at the GABA transporter GAT1. *J. Neurosci.* **16,** 5405–5414 (1996).
31. Penado, K. M., Rudnick, G. & Stephan, M. M. Critical amino acid residues in transmembrane span 7 of the serotonin transporter identified by random mutagenesis. *J. Biol. Chem.* **273,** 28098–28106 (1998).
32. Chen, N. & Reith, M. E. Na^+ and the substrate permeation pathway in dopamine transporters. *Eur. J. Pharmacol.* **479,** 213–221 (2003).
33. Mari, S. A. *et al.* Aspartate 338 contributes to the cationic specificity and to driver-amino acid coupling in the insect cotransporter KAAT1. *Cell. Mol. Life Sci.* **61,** 243–256 (2004).
34. Jardetzky, O. Simple allosteric model for membrane pumps. *Nature* **211,** 969–970 (1966).
35. Pantanowitz, S., Bendahan, A. & Kanner, B. I. Only one of the charged amino acids located in the transmembrane alpha-helices of the γ-aminobutyric acid transporter (subtype A) is essential for its activity. *J. Biol. Chem.* **268,** 3222–3225 (1993).
36. Bennett, E. R., Su, H. & Kanner, B. I. Mutation of arginine 44 of GAT-1, a $(Na^+ + Cl^-)$-coupled γ-aminobutyric acid transporter from rat brain, impairs net flux but not exchange. *J. Biol. Chem.* **275,** 34106–34113 (2000).
37. Loland, C. J., Granas, C., Javitch, J. A. & Gether, U. Identification of intracellular residues in the dopamine transporter critical for regulation of transporter conformation and cocaine binding. *J. Biol. Chem.* **279,** 3228–3238 (2004).
38. Loland, C. J., Norregaard, L., Litman, T. & Gether, U. Generation of an activating Zn^{2+} switch in the dopamine transporter: mutation of an intracellular tyrosine constitutively alters the conformational equilibrium of the transport cycle. *Proc. Natl Acad. Sci. USA* **99,** 1683–1688 (2002).
39. Toyoshima, C. & Nomura, H. Structural changes in the calcium pump accompanying the dissociation of calcium. *Nature* **418,** 605–611 (2002).
40. Lopez-Corcuera, B., Nunez, E., Martinez-Maza, R., Geerlings, A. & Aragon, C. Substrate-induced conformational changes of extracellular loop 1 in the glycine transporter GLYT2. *J. Biol. Chem.* **276,** 43463–43470 (2001).

41. Sato, Y., Zhang, Y. W., Androutsellis-Theotokis, A. & Rudnick, G. Analysis of transmembrane domain 2 of rat serotonin transporter by cysteine scanning mutagenesis. *J. Biol. Chem.* **279,** 22926–22933 (2004).
42. Stephan, M. M., Chen, M. A., Penado, K. M. & Rudnick, G. An extracellular loop region of the serotonin transporter may be involved in the translocation mechanism. *Biochemistry* **36,** 1322–1328 (1997).
43. Smicun, Y., Campbell, S. D., Chen, M. A., Gu, H. & Rudnick, G. The role of external loop regions in serotonin transport. *J. Biol. Chem.* **274,** 36058–36064 (1999).
44. Yernool, D., Boudker, O., Jin, Y. & Gouaux, E. Structure of a glutamate transporter homologue from *Pyrococcus horikoshii*. *Nature* **431,** 811–818 (2004).
45. Guerrero, S. A., Hecht, H. J., Hofmann, B., Biebl, H. & Singh, M. Production of selenomethionine-labelled proteins using simplified culture conditions and generally applicable host/vector systems. *Appl. Microbiol. Biotechnol.* **56,** 718–723 (2001).
46. Terwilliger, T. C. & Berendzen, J. Automated MAD and MIR structure solution. *Acta Crystallogr. D* **55,** 849–861 (1999).
47. Collaborative Computational Project, No. 4, The CCP4 suite: program for protein crystallography. *Acta Crystallogr. D* **50,** 760–763 (1994).
48. Perrakis, A., Morris, R. & Lamzin, V. S. Automated protein model building combined with iterative structure refinement. *Nature Struct. Biol.* **6,** 458–463 (1999).
49. Brünger, A. T. *et al.* Crystallography & NMR system: a new software suite for maclomolecular structure determination. *Acta Crystallogr. D* **54,** 905–921 (1998).
50. Yernool, D., Boudker, O., Folta-Stogniew, E. & Gouaux, E. Trimeric subunit stoichiometry of the glutamate transporters from *Bacillus caldotenax* and *Bacillus stearothermophilus*. *Biochemistry* **42,** 12981–12988 (2003).

Supplementary Information is linked to the online version of the paper at www.nature.com/nature.

Acknowledgements We appreciate the beamtime and the assistance of the personnel at beamline 8.2.2 of the Advanced Light Source and beamlines X4A, X12B and X29 of the National Synchrotron Light Source; B. Honig and L. Forrest for help with sequence alignment; M. A. Gawinowicz for mass spectrometry and free amino acid analysis; J. Moon for help with bacterial culture and crystallization; H. Furukawa for assistance with vector construction and light scattering experiments; O. Boudker for liposome reconstitution; and D. Yernool, O. Boudker and R. Ryan for comments on the manuscript. A.Y. is on leave from the Laboratory for Structural Biochemistry, RIKEN Harima Institute at SPring-8, Japan. S.K.S. is supported by an NIH NRSA postdoctoral fellowship. The work was supported by the NIH. E.G. is an investigator with the Howard Hughes Medical Institute.

Author Information The coordinates for the structure have been deposited in the Protein Data Bank under the accession code 2A65. Reprints and permissions information is available at npg.nature.com/reprintsandpermissions. The authors declare no competing financial interests. Correspondence and requests for materials should be addressed to E.G. (jeg52@columbia.edu).